Oxidation of Metals (2022) 97:209–226
https://doi.org/10.1007/s11085-021-10087-y

ORIGINAL PAPER

Protective Alumina Scale Growth at 900 °C for a Ni- and Cr-Free Co-Base Model Alloy with γ/γ′-Microstructure: Synergistic Effects by Combining Shot-Peening and Halogenation

S. P. Hagen[1] · K. Beck[2] · D. Kubacka[3] · H.-E. Zschau[2] · M. C. Galetz[2] · E. Spiecker[3] · S. Virtanen[1]

Received: 23 September 2021 / Revised: 21 October 2021 / Accepted: 22 October 2021 /
Published online: 2 November 2021

Abstract

The oxidation resistance of novel γ/γ'-strengthened Co-base superalloys is clearly outmatched by their Ni-base counterparts within the high-temperature regime. Therefore, surface modification strategies to foster protective alumina growth seem auspicious. This study elucidates the impact of fluorination and shot-peening on protective alumina formation at 900 °C for a quaternary Co-base model alloy (Co-Al-W-Ta system) which is well known for an exceptionally low inherent oxidation resistance. Time-resolved isothermal gravimetric analysis (TGA) in synthetic air, detailed electron microscopic analysis, and X-ray diffraction (XRD) were used. For polished samples, no pronounced enhancement of oxidation resistance could be obtained by halogenation. However, in case of shot-peened samples (halogen-free), an increased tendency for alumina formation is found compared to polished surfaces. The very early stages of oxidation were identified to be especially crucial with respect to sustainable protective scale growth. Most noteworthy is the observation of a strong synergistic effect derived by a combination of halogenation and shot-peening, leading to significantly increased oxidation resistance.

Keywords High-temperature oxidation · Cobalt-base superalloys · Halogen effect · Protective scales · Shot-peening · Ion implantation

✉ S. P. Hagen
sebastian.p.hagen@fau.de

Extended author information available on the last page of the article

Introduction

Gas turbine blades have to simultaneously withstand highest mechanical loads and temperatures within harsh environments [1, 2]. Due to outstanding strength and toughness, as well as good oxidation and corrosion resistance at elevated temperatures, Ni-base superalloys are the construction material par excellence for such demands [3]. To increase the efficiency of gas turbines, engineers typically target to raise the operating temperatures, as it is indicated by the modified Brayton cycle (thermodynamic cycle) [4–6]. Since the potential for an ongoing optimization of Ni-base superalloys is, however, largely exhausted, alternative materials that outmatch the temperature-limit set by current Ni-base alloys (up to 1200 °C for short-time exposure) are desirable [3, 6–8].

In 2006, Sato et al. laid the cornerstone for Co-base superalloys by discovering an ordered intermetallic phase (γ') that exhibits $L1_2$ crystal structure in the ternary Co-Al-W system. This γ'-phase (Co_3(Al,W)) can precipitate coherently within the face-centred cubic (fcc) matrix (y), resulting in a two-phase microstructure which is highly comparable to that of Ni-base superalloys [9, 10]. Initially, Co-base superalloys have been seen as highly promising alternatives, as pure Co outmatches the melting point of pure Ni by 40 °C [6–8, 11]. Even though quite remarkable mechanical properties could be achieved since 2006, the oxidation resistance of Co-base superalloys at temperatures exceeding 800 °C still undoubtedly ranks behind their Ni-base counterparts and needs to be increased for serious competitiveness [5, 12–16]. Therefore, strategies to enable the growth of protective and sustainable oxide scales, e.g. alumina or chromia, need to be found. According to Wagner's model, both a sufficient concentration and diffusivity of Al and Cr within the alloy can be identified as crucial to achieve this goal [17].

In a recent study, we demonstrated a strategy that allowed to tremendously increase the oxidation resistance of four Co-base model alloys with γ/γ'-microstructure [18]. Based on a combination of shot-peening (prior to oxidation) and a temporary exposure to oxygen deficient atmosphere (impure argon during heating), protective alumina scale growth could be achieved. In contrast, all alloys in polished surface state were prone to exceptionally high oxidation kinetics caused by massive internal oxidation and external growth of Co oxides. In accordance with other authors, it was concluded that shot-peening—and by that plastic deformation—induces additional lattice defects that can act as short circuit paths for diffusion and thereby increase the effective solute diffusivity [18–21].

When the exposure procedure abstained from heating in argon atmosphere, for shot-peened samples clearly less continuous and protective alumina scales with higher amounts of transient oxides developed [18]. In contrast, for polished samples, no significant effect of the heating atmosphere on oxidation kinetics was found [18]. Therefore, it could be concluded that the shot-peening treatment did increase the tendency of the alloys to form protective alumina scales, whereas alone, it was not sufficient to initiate the latter. For more details on the interaction of surface deformation and atmosphere, the reader is referred to [18].

A promising alternative strategy to foster protective alumina scale growth is based on the application of halogens in the surface proximity prior to oxidation. This effect was initially discovered for titanium aluminides [22, 23]. Correspondingly, this approach is typically referred to as the halogen effect. In principle, the halogen effect can be caused by various halogens; however, most promising results were obtained for fluorine [24, 25]. For applying the latter, typically, ion implantation is conducted, even though also other methods such as liquid phase immersion with diluted HF-based solutions are suitable [26, 27]. For the high-temperature exposure of halogenated samples, various gaseous metal-halide- and metal-oxy-halide-species (like: AlF, Cr_2F, TiF, NiF, FAlO) can form [28]. Even though all these compounds are volatile at high temperatures, the working mechanism of this method relies on the fact that among these species, Al-halides (e.g. AlF) possess an exceptionally high formation energy, as well as vapour pressure, and thus increase the Al activity on the surface [28]. The transport of Al-halides is supported by pores and micro-cracks that link the substrate and the overlying oxide scale. Assuming the latter to expand in through-thickness direction of the scale, an internal oxygen partial pressure gradient is originated. With increasing distance from the substrate, thus with increasing oxygen pressure within the respective cavity, the gaseous halides become progressively unstable and consequently oxidize. In case of AlF for example, the reaction depicted in Eq. (1) prevails. Thereby, both alumina and gaseous fluorine are yielded. The latter is extremely reactive and can subsequently return to the cycle [25].

$$4\mathrm{AlF}\,(g) + 3\mathrm{O}_2 \rightarrow \mathrm{Al}_2\mathrm{O}_3(s) + 2\,\mathrm{F}_2 \tag{1}$$

Even though the method was initially developed for Ti–Al alloys of which a significant improvement in oxidation resistance could be achieved [26, 29], highly promising studies on Ni-base alloys are also on hand [30–32]. A recent study on a model-alloy series (XCo-YNi-9Al-8Cr-8 W), in which the Co/Ni-ratio was systematically varied, confirmed the existence of the halogen effect for the Ni-rich alloys ($Y/X > 1$), as external alumina growth could be facilitated [33]. The results, however, indicated a diminished efficacy of the halogen effect in case of the Co-rich alloys of this series, as no external alumina scale could be generated [33].

The present study focuses on a quaternary Ni- and Cr-free Co-base model alloy of the Co-Al-W-Ta system, showing an exceptionally low oxidation resistance in polished surface state which could be improved by fostering alumina growth after applying shot-peening and heating in oxygen deficient atmosphere [18]. In the current study, to draw conclusions on the applicability and magnitude of the halogen effect for Co-base alloys, firstly, halogenation was conducted with two different intensities. Secondly, besides polished samples, also shot-peened samples were taken for halogenation, as plastic deformation was unequivocally shown to increase the tendency for lateral alumina growth and to demonstrate possible synergistic effects of shot-peening and halogenation. Following the experimental procedures and findings in our previous study [18], the exposure was conducted in synthetic air for a duration of 36 h at 900 °C by means of time-resolved isothermal gravimetric analysis (TGA). Subsequent to oxidation, scanning electron microscopy (SEM),

scanning transmission electron microscopy (STEM), and X-ray diffraction (XRD) were carried out in order to characterize the oxide scales.

Experimental Procedures

Sample Material

The Co-base model superalloy with γ/γ'-microstructure used in this work is based on the quaternary Co-Al-W-Ta system. According to its intended γ'-**V**olume **F**raction of 40%, the name "VF40" was given by Bezold et al. who initially designed the alloy as part of a larger series of which the volume fraction was systematically varied [34]. The oxidation behaviour of VF20, VF40, VF50, and VF60 was recently investigated in detail [18]. For the current study, we decided to investigate VF40 in more detail, as for this alloy, the strongest enhancement of oxidation resistance was achievable due to shot-peening (instead of polishing) prior to exposure in synthetic air at 900 °C [18]. The alloy was cast as a single crystal (SX) with a designated < 001 > orientation along the rod-axis by means of Bridgeman investment casting at the Institute of Metals Science and Technology (WTM, University of Erlangen-Nürnberg (FAU), Germany). To reduce the elemental segregations within the crystal, a two-stage heat-treatment was conducted. Therefore, a homogenization annealing of 24 h at 1350 °C was performed prior to an ageing step of 100 h at 900 °C for obtaining the desired two-phase γ/γ'-microstructure. Both, the nominal and actual compositions determined by SEM–EDX (FE-SEM, Hitachi S-4800) of the alloy are provided in Table 1.

Sample Preparation and Surface Modifications

Slices of 1 mm thickness were cut from the heat-treated rods and ground up to a grit size of 1200 SiC. Afterwards, a 9 µm diamond suspension was used for polishing. Subsequently, sample preparation was varied to obtain different surface states. In case of halogenated samples, ion implantation was performed as the last step of surface modification in order to avoid a mechanical removal of the F-enriched surface zone.

- Continued manual polishing down to 1 µm surface finish. The polishing procedure is referred to as "Pol" in the following.

Table 1 Nominal and actual elemental composition of alloy VF40. Actual composition measured by SEM–EDX

VF40	Co	Al	W	Ta
Nominal	84.4	8.8	5.7	1.1
Actual	80.6	9.5	7.4	2.5

All values in at.%

- Shot-peening with glass shot (type: MS400BT from IEPCO, Switzerland). Therefore, a pressure of 2.5 bar, a distance of approximately 2 cm, an impact angle of 90°, and a duration of 1 min for each side were applied. The shot-peening procedure is referred to as "SP" in the following.
- Fluorination via ion implantation using two different intensities.
- Low F-intensity: $I_L = 1.0 * 10^{17}$ F/cm^2
- High F-intensity: $I_H = 2.0 * 10^{17}$ F/cm^2

For halogenation beamline, ion implantation was performed using a CF_4 gas source. Therefore, an ion implanter of the Goethe University Frankfurt was operated at a voltage of 38 kV. Halogenation was performed on both sides of the samples to allow TGA investigations and is referred to as "F(I_L)" or "F(I_H)" in the following.

Via combining these procedures, overall six different samples of the alloy were manufactured for the ongoing TGA investigation: (1) Pol, (2) Pol + F(I_L), (3) Pol + F(I_H), (4) SP, (5) SP + F (I_L), (6) SP + F(I_H).

Thermogravimetric Analysis (TGA)

Time-resolved isothermal oxidation experiments with a dwell time of 36 h were performed at 900 °C in synthetic air. Therefore, a furnace from Thermconcept driven by an Eurotherm 3208 controller together with a TGA-unit from Sartorius (M25D-V) was used. Heating was performed at a rate of 10 K/min, and free cooling was allowed after the test. Gas flow rates were set to 37.5 ml/min, which equals a laminar gas velocity of about 2.37 cm/min.

For STEM analysis, 2 shot-peened samples (5 bar) were additionally short-time oxidized for dwell times of 2 min and 30 min. Following [18], for these TEM-samples, rates of 25 K/min were used to prevent an exaggerated progress of oxidation.

X-Ray Diffraction (XRD)

After the removal from the furnace, the samples were cut in half by a water-cooled low-speed saw. One half was used to perform XRD analysis and record diffraction patterns (D8 Advance, Bruker Corporation, Billerica, USA) using a Cu-cathode and a Ni-filter. The obtained spectra were compared to the PDF database.

Preparation of Cross Sections and Microscopic Characterization

One half of each sample was Ni-plated in order to allow a metallurgical preparation of cross sections without scaling and unwanted crack initiation within the oxide. Therefore, an Au layer was applied by sputtering prior to galvanostatic electroplating in a $NiSO_4$-based solution (current density of 15 mA/cm^2 for 30 min). Subsequently, again, the samples were cut in half and, finally, an ion-milling system (IM4000 from Hitachi) was used to achieve the cross sections.

Scanning electron microscopic (SEM) investigations were performed with a LYRA3 SEM from Tescan using secondary electron imaging (SE), as well as

backscattered electron imaging (BSE). The TEM lamellas were prepared, using dual-beam SEM–FIB Helios NanoLab 660. Scanning transmission electron microscopy (STEM) in High-Angle Annular Dark-field mode (HAADF) mode was used together with energy-dispersive X-ray spectroscopy to achieve a chemical analysis of the lamella. Therefore, a double-corrected FEI Titan Themis TEM that is equipped with a SuperX detector was run at 300 kV.

Results

Thermogravimetric Analysis (TGA) and Elucidation of Scale Structure

Figure 1 provides the TGA results obtained for an exposure duration of 36 h at 900 °C in synthetic air for all surface treatments. Among the polished samples (Fig. 1a), the oxidation resistance of the halogen-free sample is the worst, whereas it is slightly enhanced for samples of higher F-intensity. With respect to typical experimental reproducibility, no significant impact is revealed.

Comparing Fig. 1a with b, it is obvious from an oxidation point of view that also in a F-free state, all polished samples (a) rank behind their shot-peened counterparts (b). This qualitative difference between the halogen-free samples (black curves, square symbols) was expected, as the plastic deformation via shot-peening was shown to unequivocally increase the tendency of this alloy to alumina formation [18]. In contrast to polished samples (Fig. 1a), in case of shot-peened samples (Fig. 1b), a much stronger impact of halogenation on the oxidation kinetics could be identified.

In order to substantiate the TGA results, in the following, the respective SEM micrographs are discussed. In case of polished samples (Fig. 2), no qualitative differences can be observed between bare and halogenated state. According to the top view micrographs taken in SE-mode, the surface oxide structure (depicted in

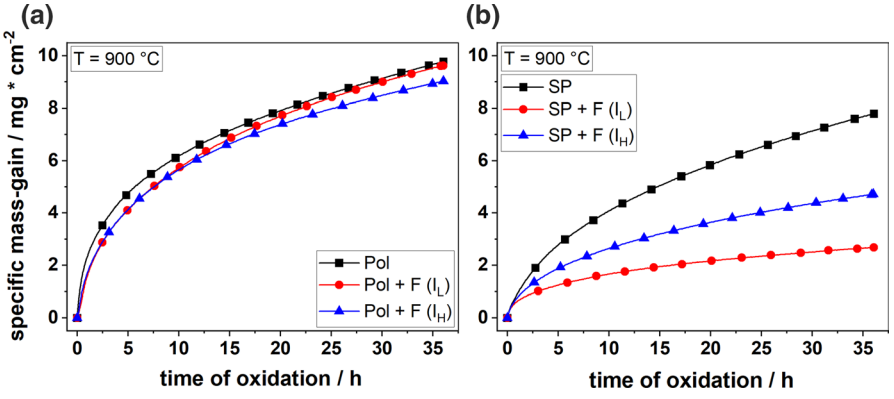

Fig. 1 Influence of surface modification (SP, Pol, $F(I_L)$, $F(I_H)$) on continuous specific mass-gain (mass-gain per surface area) at 900 °C. (**a**) depicts the results of all polished samples and (**b**) the results of the shot-peened samples

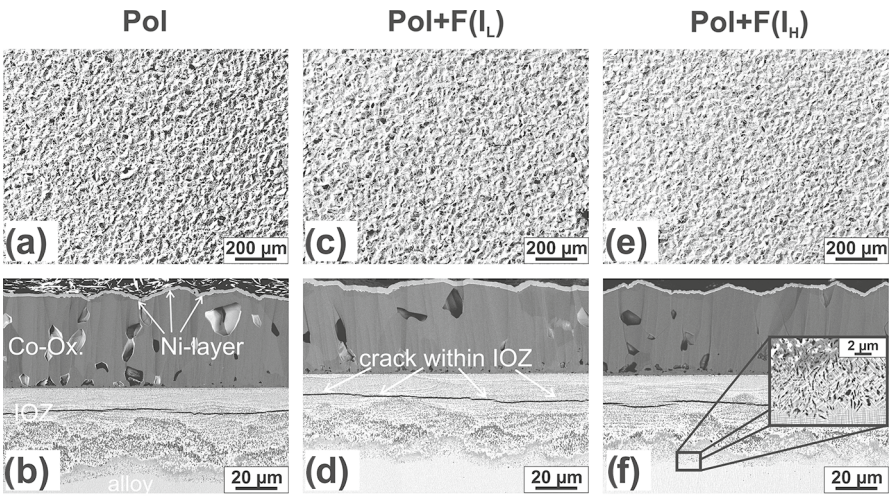

Fig. 2 Representative SEM micrographs of polished samples after 36 h exposure at 900 °C to synthetic air. With a and b for the halogen-free sample ("Pol"), c and d for "Pol + F (I_L)", and e and f for "Pol + F(I_H)." The upper row (**a**, **c**, and **e**) depicts the top view micrographs (SE), whereas the lower row (**b**, **d**, and **f**) depicts cross sections (BSE)

Fig. 2a, c and e) appears highly homogeneously distributed along the surface. All cross sections (Fig. 2b, d, and f) show a scale structure that was already explored in [18]. The characteristic zones are exemplarily labelled in Fig. 2b. A massive external Co oxide scale with significant porosity can be found as the outermost oxide layer (beneath the metallic Ni-layer that is applied in the course of sample preparation). It is noteworthy that the porosity is more pronounced in case of the F-free sample (Fig. 2b). However, to describe this effect quantitatively, further statistical analysis would be required. In Fig. 2f on the left, it can be seen that one oxide grain continues beyond the big pore. Therefore, a 3 D analysis would be required, which however is beyond the scope of this study. Underneath the Co oxide scale, an internal oxidation zone (IOZ) is developed in which distinct alumina precipitates prevail. Within the IOZ, lateral cracks can be seen (exemplarily marked in Fig. 2d). In accordance with [18], it can be expected that the latter develop during the mechanical cutting due to the evidently high porosity in this scale region. It is noteworthy that the thickness of the IOZ is slightly thinner in case of the halogenated samples. However, for none of the polished samples, dense alumina scales can be identified, not even in Fig. 2f, even though this sample (Pol + F (I_H)) was the most promising according to TGA (Fig. 1a). It can be seen in Fig. 2f that the IOZ is separated from the unaffected alloy by a 3-phase zone in which alumina precipitates are embedded within γ- and Co_3W-phase. Due to a depletion of Al, no γ'-precipitates exist in this region [18].

Overall, the results of the polished samples show that the performed halogenation procedures were insufficient to foster any continuous alumina scale formation. However, for both halogenated samples, mass-gains lower than for the F-free sample prevail and hence a slightly positive impact of fluorination can be concluded.

In case of shot-peened samples (Fig. 3), it is noteworthy that rather inhomogeneous oxide scales developed, as highlighted by means of black arrows within top view micrographs (a, d, and g). The two groups of arrows each do not refer to a precise position but rather to representative regions where either thick or rather thin scales grew. In the following, these regions are referred to as "thick spot(s)" (b, e, and h) and "thin spot(s)" (c, f, and i), respectively.

Shot-Peened Surface State

The vast majority of the halogen-free, shot-peened sample, that is depicted in Fig. 3a, b, and c, is covered by a thick oxide layer (b). As shot-peening alone was not expected to trigger protective alumina formation, this finding is in-line with a weight gain that is not much different from the polished sample (see Fig. 1). The scale appearance in Fig. 3b qualitatively represents the structure described in [18] for solely shot-peened samples: Beneath an outer Co oxide scale that is prone to a considerable degree of porosity, an IOZ can be found. Within the latter, distinct alumina precipitates prevail. At a certain depth within the IOZ, the inset of

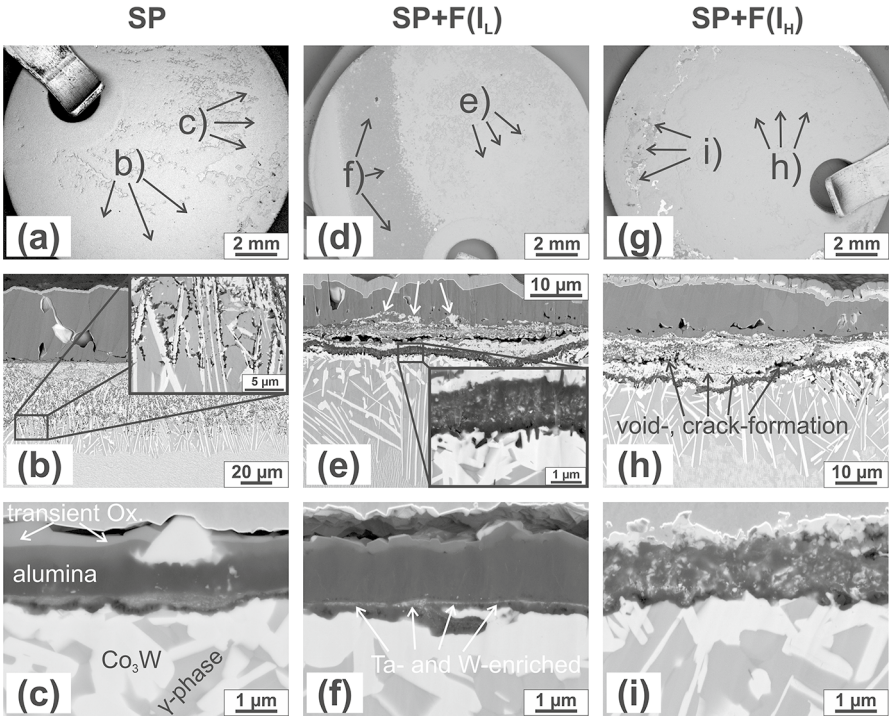

Fig. 3 SEM micrographs of shot-peened samples after 36 h exposure at 900 °C to synthetic air. With a, b, and c for the halogen-free sample ("SP"), d, e, and f for "SP + F(I_L)", and g, h, and i for "SP + F(I_H)." The upper row (**a**, **d**, and **g**) depicts the top view, the middle row (**b**, **e**, and **h**) depicts cross sections of the thick spots, and the lower row (**c**, **f**, and **i**) depicts cross sections of the thin spots (BSE)

Co_3W-formation can be recognized. The facilitated formation of this W-rich phase compared to the polished counterpart (Fig. 2b) was interpreted as a consequence of enhanced Al-depletion due to shot-peening and of the limited phase stability of the Co-base system [18]. It is noteworthy that the alumina growth is deflected along the rod-like TCP-phases towards the oxidation front, as highlighted in Fig. 3b. The spatial arrangement of the large intermetallic rods obviously impedes the growth of a lateral protective alumina scale, as the TCP-phase penetrates deeper into the alloy than the oxidation front. Overall, one can conclude that after an exposure duration of 36 h, due to massive formation and spatial arrangement of the Co_3W-phase, an unpromising situation with respect to lateral alumina scale growth prevails. As a sufficient Al-depletion is a prerequisite for Co_3W-formation, one may ask if also during the very early stages ($t < 36$ h) of oxidation TCP-phases hamper a continuous alumina formation.

Therefore, two shot-peened samples were additionally short-time exposed for 2 min (Fig. 4a and c) and 30 min (Fig. 4b and d) at 900 °C in synthetic air and subsequently taken for STEM-EDX analysis. Lamellas were prepared from those spots, where the formation of unprotective (thick) Co oxides was found. The results reveal that already after short duration (2 min), a considerable amount of Co oxides was formed as the outermost layer. The composition of the latter was determined at position (1) in Fig. 4a and is shown in Table 2. Underneath the latter, an IOZ can be found that is comprised of various oxides, highlighted as position (2) in Fig. 4 (see Table 2). The IOZ shows a sharp border towards the depletion affected alloy by an Al-enriched oxide layer (Fig. 4c and position (3) in Table 2). A sudden change in oxygen content when crossing this Al-rich zone suggests that it highly limits diffusion. Underneath the oxide, the depletion affected alloy with Co_3W-formation (position (4) in Table 2) can be found, what was not necessarily expected after this comparably short exposure duration. However, in contrast to the cross section obtained after an exposure time of 36 h, no impact of the Co_3W-phase on the progress of the internal oxidation front can be seen. It is noteworthy that the Co_3W phase did not form the typical rod shape, but has much lower aspect ratios. This finding clearly indicates that the deflection of the internal oxidation front through the spatial arrangement of the TCP-rods, as it was described for the 36 h experiments, cannot be directly seen as a reason for the absence of lateral alumina scale growth.

The STEM results for the sample of an exposure duration of 30 min (Fig. 4b and d) depict an Al-enriched lateral oxide layer, highlighted by white arrows within the Al-distribution map, that is highly comparable to the one described in case of the 2 min sample. However, an ongoing internal oxidation underneath this aforementioned layer indicates an insufficient barrier effect. In contrast to Fig. 4c, after 30 min of exposure, alumina formation is deflected by γ/γ-grain boundaries (and not along γ/Co_3W-interfaces) that formed due to recrystallization. The latter is exemplarily highlighted within the respective Al-distribution map by means of a white ellipse (Fig. 4d). It is noteworthy that also Co_3W precipitates are more probable to nucleate along the grain boundaries. It is assumed that the thickness of the recrystallisation zone in case of samples that were oxidized for 36 h (see Fig. 3b) determines the position within the IOZ below which the inset of large Co_3W rods can be recognized.

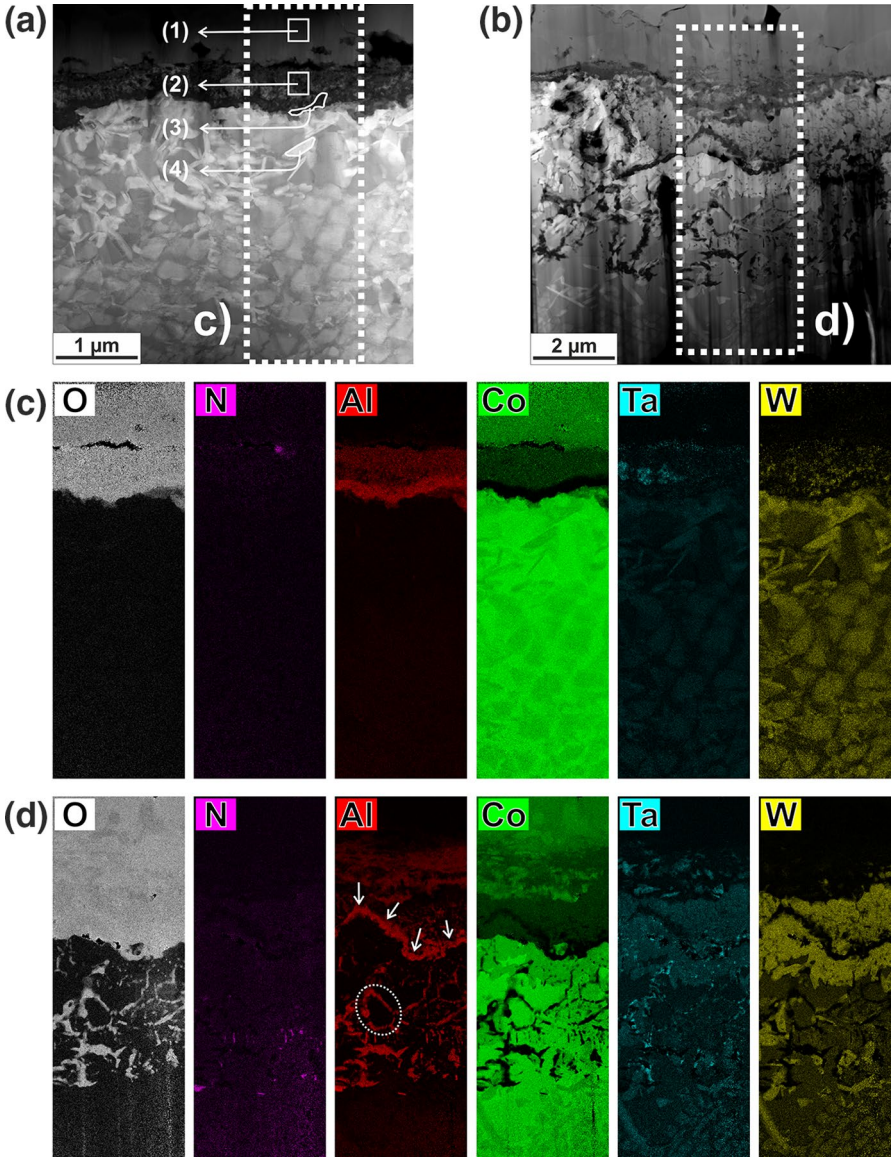

Fig. 4 Investigations of oxide scales grown on halogen-free shot-peened samples during oxidation at 900 °C in synthetic for 2 min (**a** and **c**) and 30 min (**b** and **d**) duration. Positions of elemental distribution maps (STEM-EDX) depicted in c and d are marked by white rectangles within **a** and **b** (STEM-HAADF). The compositions of the numbered regions marked in a are provided in Table 2

Last but not least, it needs to be mentioned that, especially for the 30 min sample, nitride (AlN) formation close to the IOZ is found. That means that a considerable inward nitrogen flux must prevail during the early stages of oxidation. As the formation of nitrides may lead to trapping of Al, this process can be expected to lower

Table 2 STEM-EDX measurement of the elemental concentration within the highlighted (numbered) areas in Fig. 4a in at. %

Position	Description	O	Al	Co	Ta	W
(1)	CoO	52.7	0.2	47.1	0	0
(2)	mixed oxides	58.3	19.5	17.7	1.9	2.6
(3)	Al_2O_3	59.1	37.5	0.8	1.7	0.9
(4)	Co_3W	0.8	1.2	79.7	2.7	15.6

the probability for lateral alumina growth [35]. After the thick spot was discussed so far, in the following, the thin spot of the shot-peened sample (Fig. 3c) shall be elucidated. The latter is covered only by a tiny outer scale of transient oxides that is marked exemplarily in Fig. 3c (it is even less pronounced in f and i). Within the alumina scale, according to STEM results that will be provided later within the manuscript, Ta- and W-enriched phases are embedded. This is exemplarily highlighted in Fig. 3f. A striking qualitative difference compared to Fig. 3b is the total omission of any IOZ underneath the alumina scale (Fig. 3c, f, and i). Therefore, locally, a high protectiveness of the alumina scales can be concluded.

Shot-Peened and Halogenated Surface State F(I_L)

The structure of the thick spot of the F-implanted sample (Fig. 3e) clearly differs from its halogen-free counterpart. In fact, again the porous outermost oxide layer mostly consists of Co oxides, however, its way smaller thickness compared to Fig. 3b indicates a shorter transient stage of oxidation. A further difference compared to the halogen-free samples is the existence of bright oxide phases that are embedded within the outer oxide scale, exemplarily highlighted via white arrows in Fig. 3e. Underneath the outer oxide scale, an IOZ can be found that possesses a tremendous degree of pores. These pores are typically interconnected, either directly or via cracks in between as highlighted in Fig. 3h. In contrast to the F-free sample (Fig. 3b), the IOZ of the halogenated samples shows a sharp border towards the subjacent Al-depleted zone via a horizontal Al-rich layer, appearing dark in the BSE-micrographs which is exemplarily highlighted in Fig. 3e. Neither within nor beyond this dark layer, any rod-like traces of Co_3W-phase can be seen; however, clearly, phases other than alumina are embedded. Beneath this dark layer, some alumina pegs and also distinct precipitates can be detected within a zone of approximately 1 µm thickness (highlighted region of Fig. 3e). Compared to the respective region that is depicted in Fig. 3b, this limited width clearly outlines the diffusion limiting properties of the alumina-enriched layer that evolves in case of the halogenated sample.

In contrast to Fig. 3a, where the vast majority of the surface was covered by unprotective thick Co oxide scales, in Fig. 3d, a very localized dark region is eye-catching which is highly geometrically restraint. Since the shot-peening jet is not very focused (diameter of approximately 1 cm in a distance of 2 cm between nozzle and sample), we believe that a slightly different halogenation intensity is responsible for this artefact. Even though the BSE-contrast strongly suggests that

this area might be alumina dominated, a STEM-lamella was prepared (Fig. 5) to allow a detailed chemical analysis via EDX.

The results provided in Fig. 5 confirm that indeed a partially compact alumina scale was formed. It is noteworthy that it possesses an increasing amount of porosity in inward direction. Within the compact part of the alumina scale, bright phases (STEM-HAADF) are embedded that are aligned along oxide grain boundaries. According to the element distribution maps along these lines, only partially, both F and Co enrichment prevail. In contrast, at some of these bright hairlines, mainly, one of both elements could be detected. This is especially noteworthy in case of the strong enrichment marked by arrows within the Co distribution map that is not at all depicted for F. Additionally, within the F-map, a grain boundary is marked at which no increasing Co content is found.

Whereas solely negligible enrichments of Ta and W could be identified along the grain boundaries of the upper and compact part of the alumina scale, refractory metals strongly accumulate within the porous scale section underneath (see also Fig. 3f). A preferential spreading along grain boundaries cannot be detected in this region. Obviously, the F-distribution matches well to the Ta and W enrichments. Additionally, the fluorine content is enlarged along the border between the dense upper and the porous lower scale section.

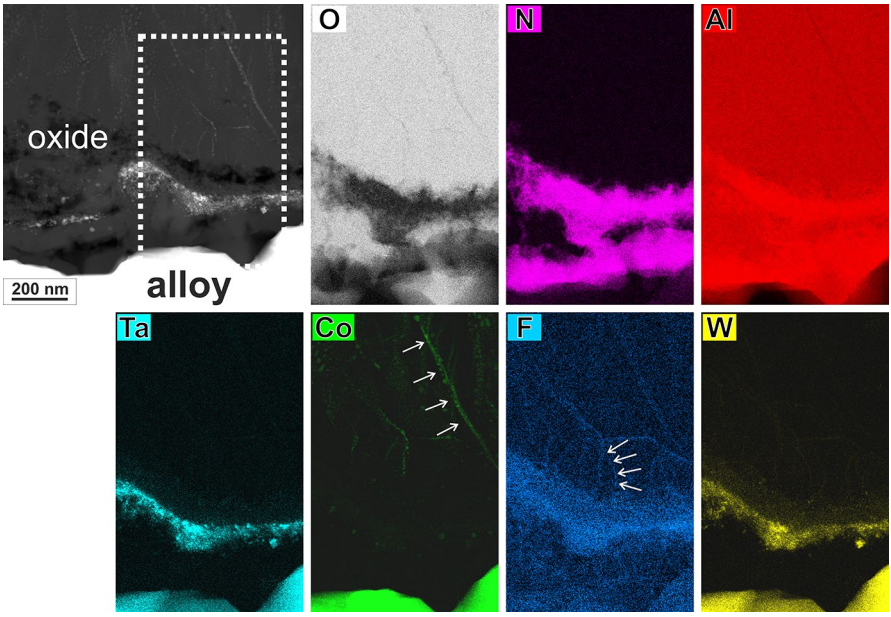

Fig. 5 Elemental distribution at the oxide/alloy-interface of SP + F(I_L) after oxidation for 36 h at 900 °C in synthetic air. a depicts a STEM-HAADF micrograph in which the position of the elemental distribution maps is marked by a white rectangle (dashed line)

Shot-Peened and Halogenated Surface State F(I_H)

In contrast to the lower intensity halogenation (Fig. 3d), the samples halogenated with the higher intensity lead to a comparably even oxide on the surface (Fig. 3g). Only few dark alumina spots can be found. Additionally, bright areas prevail in Fig. 3g that are caused by local spallation of the outer oxide scale.

The scale structure at the thick spots (Fig. 3h) does not reveal any qualitative difference to the shot-peened sample halogenated with the lower intensity (e).

The cross section of the thin spot (Fig. 3i), however, obviously differs from its halogen lean counterparts (c and f). In case of the latter, Ta- and W-rich oxides are embedded within a horizontal region of confined thickness, only. In case of high fluorination intensity (Fig. 3i), the occurrence of a massive amount of embedded bright phases throughout the entire oxide scale is noteworthy. Even though the composition of these oxide phases has not been confirmed for this sample, according to BSE-contrast and the STEM-EDX analysis depicted in Fig. 5, it can be concluded that Ta and W oxides prevail, too.

This assumption is further substantiated when comparing the micrographs depicted in Fig. 3c and f with i, regarding the Co_3W formation. Whereas in case of both the F-free samples and the sample halogenated with low F-intensity (Fig. 3c and f), a pronounced accumulation of Co_3W-phase along the interface "oxide/depletion zone" is visible, in case of a higher fluorine level (Fig. 3i), a much larger amount of γ-phase is formed along that interface. This might be a consequence of extensive formation of gaseous halides, due to a too high F-intensity. As a result, elements other than Al (e.g. W, Ta) are present within the alumina scale and simultaneously the growth of W- and Ta-rich TCP-phases along the interface "oxide/depletion zone" is impeded.

XRD Results

As the provided results so far only reveal information of highly confined parts of the samples (ion-milling based cross sections and STEM-lamellas), additionally, X-ray diffraction (XRD) was performed (see Fig. 6). The results indicate an increasing tendency of alumina formation with shot-peening and additional halogenation as compared to polished surface state. In case of the polished sample, besides Co_3O_4 and CoO also spinel-phase (Co_2AlO_4) was identified. In case of the shot-peened sample and additionally fluorinated sample, exclusively, alumina formation could be observed.

Discussion

So far, a detailed description of the individual results was conducted. In the following, the results are briefly summarized to allow an overall discussion of the findings.

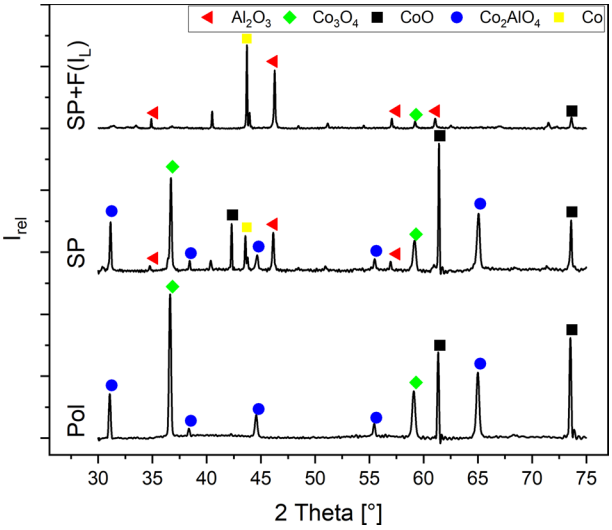

Fig. 6 X-ray diffraction (XRD) patterns of oxidized samples (36 h, 900 °C synthetic air) differing in surface state prior to oxidation. Bottom: Pol, middle: SP, top: SP + F(I_L)

For all polished samples, massive oxidation rates were detected. Neither for halogen-free nor for fluorinated samples of polished surface state, continuous alumina scale growth could be initiated. The mechanism for polished and halogen-free surface state was investigated in detail by means of STEM and SEM analyses in [18]. As both the scale structures and the oxidation kinetics for polished samples are all highly comparable, the mechanism proposed for internal alumina formation [18] is not expected to be significantly affected by halogenation. Following [18], this means that during the early stages of oxidation, alumina nucleation at the Internal Oxidation Front (IOF) is mainly restricted to the γ-phase. Since Al-transport towards the alumina precipitates was identified to be slow, no sufficient lateral growth that was needed for the transition to continuous layer formation can take place [18, 36]. The halogen effect turned out to slightly decrease the mass-gain after 36 h of exposure in case of polished samples (relative reduction of 7.5%). Since no statistic evaluation of the alumina precipitate size was conducted, it cannot be excluded that this difference might be based on a slight coarsening of the distinct alumina precipitates [37] that is simply not clearly depicted within the ion-milling-based cross sections. Also, an increased internal formation of spinel phase due to halogenation might contribute to the enhancement in oxidation resistance [31]. Accordingly, here, for instance, Co_2AlO_4 was detected by XRD for all polished samples. In contrast to the Co-base alloy used in this work, results available in the literature for Ni-base alloys reveal a much higher effectiveness for the halogen effect. For instance, Zschau et al. reported a change from discontinuous to protective alumina scale growth for alloy IN738 at 1050 °C. This is remarkable, since the Al content of IN738 is by far lower compared to the here investigated Co-base alloy (6.7 at.% vs. 9.5 at.%) [28, 32]. The order of oxidation resistance among the polished samples indicates that the application of

even higher F-levels might be beneficial in case of Co-base alloys. The latter is an interesting outcome, as results for some Ni-base alloys indicated $F(I_H)$ to be already beyond (or at least close) to the threshold value for a positive halogen effect [31]. We assume that the massive internal oxidation in polished surface state, leading to a highly porous IOZ, contributes to a rapid loss of halides and therefore to a fast decay of the F-effect efficacy. The latter can be concluded, since the overlying Co oxide scale does not provide a sufficient barrier function. This is in accordance with [32] where a significant loss of fluorides within the subsurface region of IN738 is described to attenuate due to the growth of a continuous alumina scale.

Shot-peening prior to exposure was identified to increase the tendency of the investigated Co-base superalloy for protective alumina scale formation [18]. In halogen-free state (see Fig. 3a), the great majority of the sample surface was still prone to the massive unprotective oxide growth. Only at a few localized regions, a continuous outer alumina scale growth was successfully achieved. This in fact is the intended outcome for our experimental design, as shot-peening should not lead to continuous alumina formation (idea of "leaving work for the halogen effect"). Indeed, through halogenation, the fraction of the surface covered by protective alumina could be clearly increased (see Fig. 3d), unequivocally confirming the existence of the halogen effect for the here studied Cr-free Co-base alloy. To better understand the cause of this improvement, the early stages of scale formation in case of halogen-free shot-peened samples were investigated in detail by means of STEM-EDX. Therefore, lamellas were prepared from those spots, where thick scales predominated, i.e. where no protective alumina formation was achieved by shot-peening. The results indicate that at these spots, a "critical stage" for continuous alumina formation occurs during exposure. This means that initially, indeed a lateral Al-rich barrier layer is formed also at the thick spots, which effectively hinders the inward diffusion of oxygen. Accordingly, at this stage, no internal oxidation can be found underneath this zone. However, the STEM micrographs taken for a longer exposure duration (30 min instead of 2 min) clearly show the breakdown of the initially formed barrier layer. Internal oxidation, penetrating into the alloy along alloy grain boundaries, can be found and is a remarkable difference to results of extended exposure durations, as there the IOF is typically deflected along the γ/Co_3W-interfaces (see Fig. 3b). Since plastic deformation induces an initial tendency for protective layer formation ("critical stage"), that is not existent in case of polished samples, the halogen effect could be shown to be sufficient to trigger protective alumina scale growth. The latter effectively prevents the inward diffusion of oxygen up to an exposure duration of at least 36 h at 900 °C (see Fig. 3f and i). Until now, the role of such a continuous alumina scale in preventing gaseous halide loss and stabilizing the halogen effect for longer exposure durations has already been described for a Ni-base alloy [32]. In the current work, for the first time in the context of the halogen effect, a F enrichment along the alumina grain boundaries was detected (see Fig. 5). The latter indicates a partial loss of fluorine from the "halogen-effect-cycle" not only during temperature ramp-up [32], but also during steady state oxidation. This means that a decay of the halogen effect over time is projected in case of Co-base alloys. It should be mentioned that also in the halogenated

surface state, external alumina growth still did not spread along the entire surface. Whether at a certain spot ultimately a protective scale develops or not might be determined by a complex interplay of various factors. The conducted shot-peening treatment effectuates the alloy to be at the border to alumina formation and therefore to be highly susceptible even to minor influences (through which in case of polished surface state only a negligible variation in oxide thickness was provoked). For example, small local differences regarding the halogenation intensity, the occurrence of deformation-induced defects like cracks, or local compositional variations caused by residual solidification-induced segregations might play a role. Therefore, final conclusions on the impact of fluorination intensity for shot-peened samples should not be drawn on the basis of the presented data. Even though still thick oxide spots remained growing, through a combination of halogenation and shot-peening, a relative decrease of 65.5% in mass-gain could be achieved (comparing the mass-gain after 36 h of "SP" and "SP + F(I_L)").

Conclusions

The effect of fluorination on the high-temperature oxidation resistance of a Co-base model alloy with γ/γ'-microstructure (Co-Al-W-Ta system) was investigated. For this, samples with polished and shot-peened surface states were F-ion-implanted using two different intensities and exposed at 900 °C in air for 36 h (time-resolved isothermal thermogravimetric analysis, TGA). The scale formation was elucidated by means of detailed electron microscopic analyses and X-ray diffraction (XRD). The following conclusions can be drawn:

- Halogenation was not capable to trigger protective alumina formation in case of a polished surface state. Unprotective external Co oxide scales of significant thickness and massive internal oxidation led to very high oxidation kinetics, comparable to the halogen-free state.
- Shot-peening prior to exposure significantly enhanced the oxidation resistance of the halogen-free samples. Very locally, an outer alumina barrier was found after 36 h of exposure in case of halogen-free shot-peened samples. However, in large parts, the system could not form protective alumina scales.
- A synergetic effect of shot-peening-induced surface deformation and fluorination to strongly improve the oxidation resistance was found. Firstly, the fraction of the surface covered by protective alumina strongly increased compared to halogen-free shot-peened samples. Secondly, even at the spots, where oxides other than alumina formed, the thickness of the scale still decreased.

Acknowledgements Scientific and financial support by the Deutsche Forschungsgemeinschaft (DFG) through the Collaborative Research Center SFB-TR 103 (Project A5 and A7) is highly acknowledged.

Funding Open Access funding enabled and organized by Projekt DEAL.

Data Availability The datasets generated during and/or analysed during the current study are available from the corresponding author on reasonable request.

Declarations

Conflict of interest The authors have no relevant financial or non-financial interests to disclose.

References

1. A. Sato, Y.-L. Chiu, R. C. Reed, *Acta Materialia* **59**, 225–240 (2011).
2. T. M. Pollock, A. S. Argon, *Acta Metallurgica et Materialia* **40**, 1–30 (1992).
3. T. M. Pollock, S. Tin, *Journal of Propulsion and Power* **22**,361–374 (2006).
4. A. M. Y. Razak, 11 - Gas turbine performance modelling, analysis and optimisation. In: Jansohn P, ed. *Modern Gas Turbine Systems*. Woodhead Publishing; 2013:423–514. doi:https://doi.org/10.1533/9780857096067.3.423.
5. H.-Y. Yan, V. A. Vorontsov, D. Dye, *Corrosion Science* **83**, 382–395 (2014).
6. C. H. Zenk, I. Povstugar, R. Li et al., Acta Materialia **135**, 244–251 (2017).
7. S. Neumeier, H. U. Rehman, J. Neuner et al., *Acta Materialia*. **106**, 304–312 (2016)
8. B. A. Pint, J. R. DiStefano, I. G. Wright, *Materials Science and Engineering: A* **415**, 255–263 (2006).
9. J. Sato, T. Omori, K. Oikawa, I. Ohnuma, R. Kainuma, K. Ishida, *Science* **312**, 90–91 (2006).
10. S. Makineni, M. Singh, K. Chattopadhyay, *Annual Review of Materials Research* **51** (2021).
11. J. Yu, C. Wang, Y. Chen, C. Wang, X. Liu, *Materials & Design*. **195**, 108996 (2020).
12. L. P. Freund, S. Giese, D. Schwimmer, H. W. Höppel, S. Neumeier, M. Göken, *Journal of Materials Research* **32**, 4475–4482 (2017).
13. S. Neumeier, L. P. Freund, M. Göken, *Scripta Materialia* **109**, 104–107 (2015).
14. T. M. Pollock, J. Dibbern, M. Tsunekane, J. Zhu, A. Suzuki *JOM*. **62**, 58–63 (2010).
15. C. A. Stewart, R. K. Rhein, A. Suzuki, T. M. Pollock, C. G. Levi, OXIDE SCALE FORMATION IN NOVEL γ-γ' COBALT-BASED ALLOYS. *in Proceedings of the 13th International Symposium on Superalloys*, 991–999 (2016).
16. A. Roy, M. P. Singh, S. M. Das, S. K. Makineni, K. Chattopadhyay, *Metallurgical and Materials Transactions A* ;**52**, 5004–5015 (2021).
17. C. Wagner, *Zeitschrift für Elektrochemie, Berichte der Bunsengesellschaft für physikalische Chemie* **63**, 772–782 (1959).
18. S. P. Hagen, M. Weiser, D. Kubacka, E. Spiecker, S. Virtanen, *Oxidation of Metals*. **94**, 477–503 (2020).
19. S. Leistikow, I. Wolf, H. J. Grabke, *Materials and Corrosion*. **38**, 556–562 (1987).
20. H. J. Grabke, E. M. Muller-Lorenz, S. Strauss, E. Pippel, J. Woltersdorf, *Oxidation of Metals*. **50**, 241–254 (1998).
21. F. Wang, *Oxidation of Metals* **48**, 215–24 (1997).
22. M. Kumagai, K. Shibue, M.-S. Kim, M. Yonemitsu, *Intermetallics* **4**, 557–566 (1996).
23. M. Schütze, M. Hald, *Materials Science and Engineering: A* **239–240**, 847–858 (1997).
24. P. J. Masset, M. Schütze, *Advanced Engineering Materials* **10**, 666–674 (2008).

25. H.-E. Zschau, M. Schütze, Potential of the Halogen Effect for the Formation of a Protective Alumina Scale on Ni-Base Superalloys. In: *Superalloys 2012*. John Wiley & Sons, Ltd, 733–739 (2012) doi:https://doi.org/10.1002/9781118516430.ch81.
26. H.-E. Zschau, V. Gauthier, G. Schumacher et al., *Oxidation of Metals*. **59**, 183–200 (2003).
27. M.-H. Mo, L.-K. Wu, H.-Z. Cao, J.-P. Lin, G.-Q. Zheng, *Applied Surface Science* **407**, 246–254 (2017).
28. H. Zschau, D. Renusch, P. Masset, M. Schütze, *Materials at High Temperatures*, **26**, 85–89 (2009).
29. H.-E. Zschau, M. Schütze, H. Baumann, K. Bethge, *Intermetallics*. **14**, 1136–1142 (2006).
30. H.-E. Zschau, P. J. Masset, M. Schütze, *{ECS} Transactions*. **25**, 21–30 (2019).
31. H.-E. Zschau, W. Zhao, S. Neve, B. Gleeson, M. Schütze, *Oxidation of Metals* **83**, 335–349 (2015).
32. H.-E. Zschau, M. Schütze, M. C. Galetz et al., *Materials and Corrosion* **68**, 220–227 (2017).
33. M. Weiser, M. C. Galetz, H.-E. Zschau et al., *Corrosion Science*. **156** 84–95 (2019)
34. A. Bezold, N. Volz, F. Xue, C. H. Zenk, S. Neumeier, M. Göken, *Metallurgical and Materials Transactions A* **51**, 1567–1574 (2020).
35. U. Krupp, H.-J. Christ, *Metallurgical and Materials Transactions A* **31** 47–56 (2000).
36. D. Kubacka, M. Weiser, E. Spiecker, *Corrosion Science 191*, 109744 (2021).
37. W. Zhao, Y. Kang, J. M. A. Orozco, B. Gleeson, *Oxidation of Metals* **83**, 187–201 (2015).

Authors and Affiliations

S. P. Hagen[1] · K. Beck[2] · D. Kubacka[3] · H.-E. Zschau[2] · M. C. Galetz[2] · E. Spiecker[3] · S. Virtanen[1]

K. Beck
katharina.beck@dechema.de

D. Kubacka
dorota.kubacka@fau.de

H.-E. Zschau
dr.zschau@hotmail.com

M. C. Galetz
mathias.galetz@dechema.de

E. Spiecker
erdmann.spiecker@fau.de

S. Virtanen
virtanen@ww.uni-erlangen.de

[1] Chair for Surface Science and Corrosion, Friedrich-Alexander Universität Erlangen-Nürnberg, 91058 Erlangen, Germany

[2] DECHEMA-Forschungsinstitut, Theodor-Heuss-Allee 25, Frankfurt am Main, Germany

[3] Institute of Micro- and Nanostructure Research (IMN) and Center for Nanoanalysis and Electron Microscopy (CENEM), Friedrich-Alexander Universität Erlangen-Nürnberg, 91058 Erlangen, Germany